Electronic Supplementary Information

Enriching surface oxygen vacancies of spinel Co_3O_4 to boost H_2O adsorption for HER in alkaline media

Ting Zhu, *[a] Jun Pan,[a] Ying Xiao,[a] Anqiang Pan[a] and Shuquan Liang*[a]

[a] School of Materials Science & Engineering, Central South University, Changsha 410083, Hunan, China.

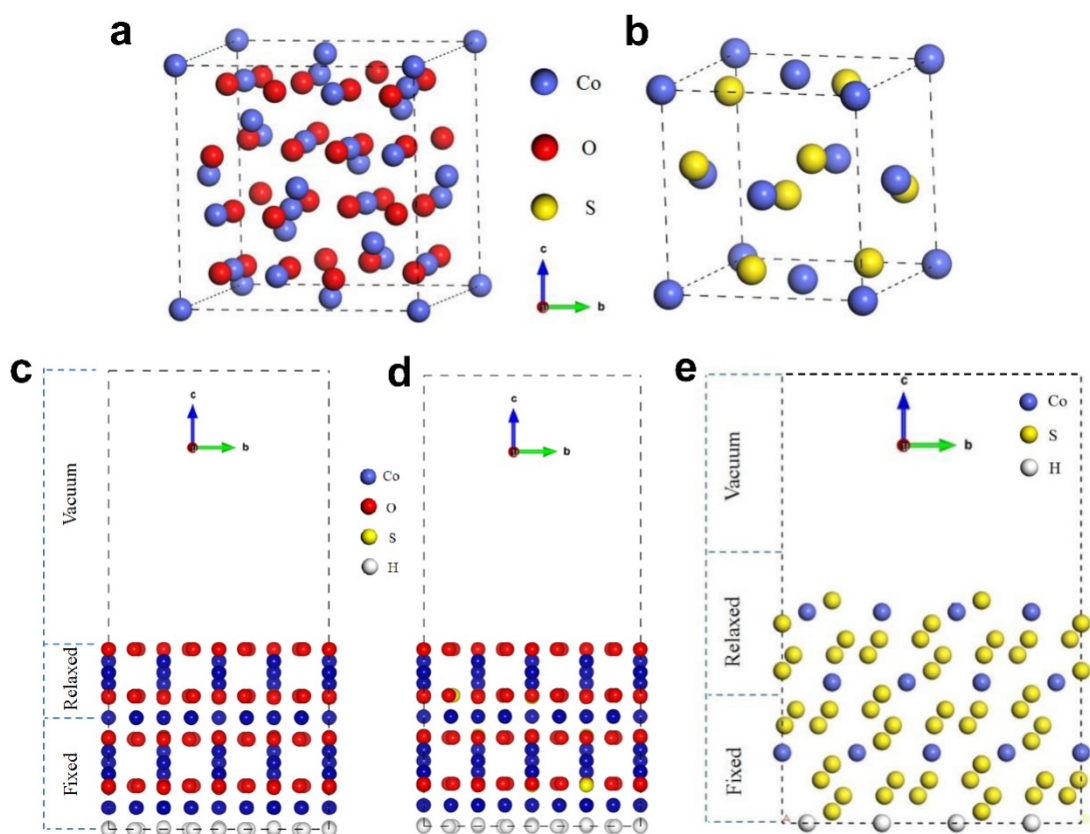*Email: zhut0002@csu.edu.cn (T. Zhu); lsq@csu.edu.cn (S. Q. Liang)*

Fig. S1. Simulation models: bulk lattice structures of Co_3O_4 (a) and CoS_2 (b); Co-O terminals of Co_3O_4 (111) (c) and $CoO_{0.88}S_{0.11}$ (111) (c), and Co-S terminal CoS_2 (111) (e).

Based on the bulk lattice structures of Co_3O_4 and CoS_2, a vacuum layer of 15 Å was added to exclude the periodic boundary interference in Z axis. The H layers at the bottom were added to remove the interference from surface Co-O or Co-S terminals.
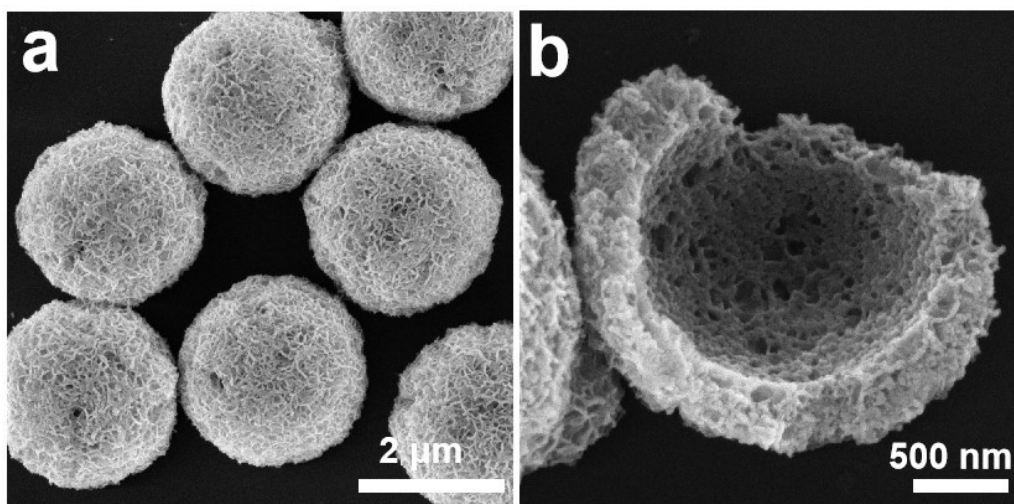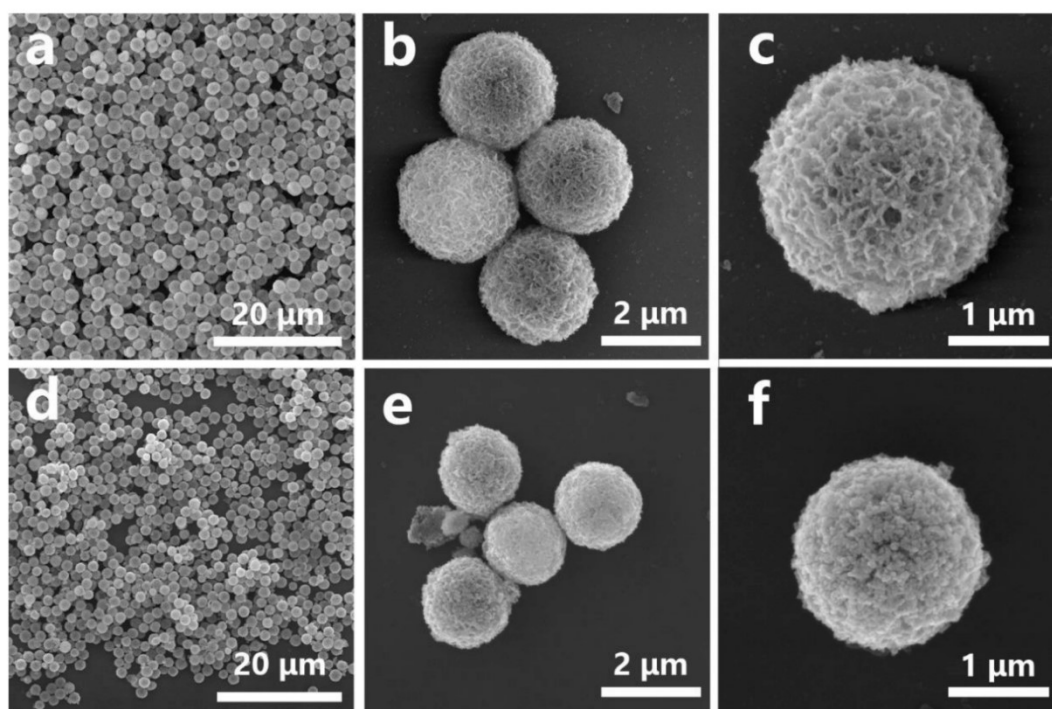
Fig. S2. SEM images of the CBP PS.

Fig. S3. SEM images of the Co$_3$O$_4$ (a-c) and CoS$_2$ (d-e) derived from CBP PS.
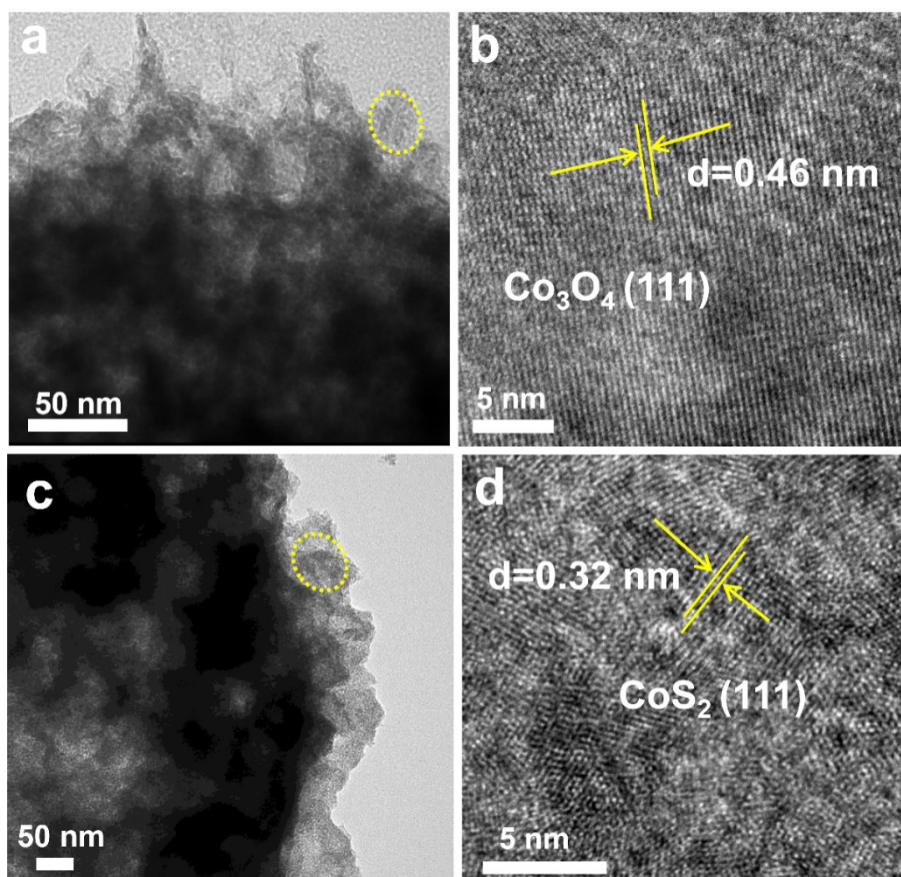
Fig. S4. TEM (a, c) and HR-TEM (b, d) images of the Co_3O_4 (a, b) and CoS_2 (c, d).

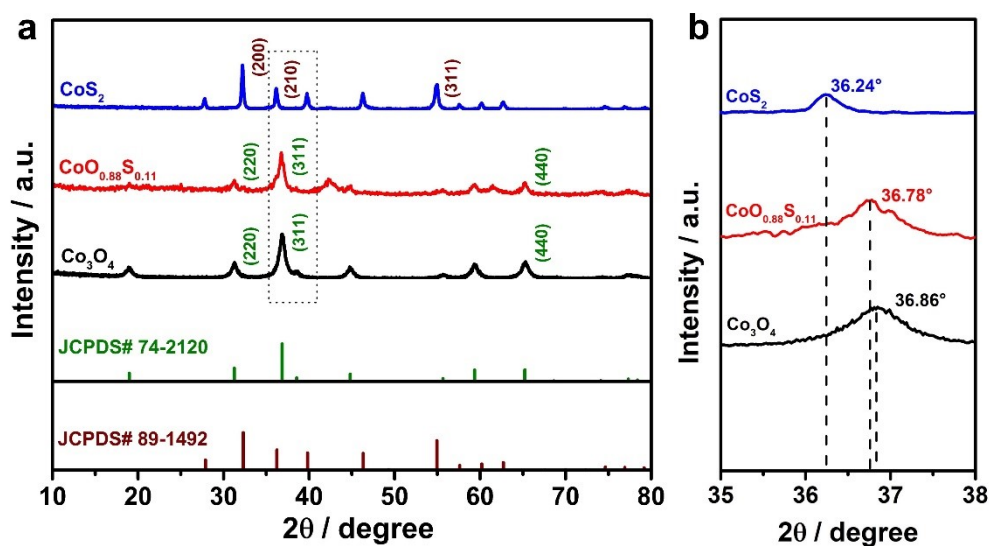**Fig. S5.** XRD patterns of the as-synthesized CoS_2, $CoO_{0.88}S_{0.11}$, and Co_3O_4 samples.

The XRD peak of Co_3O_4 (311) was shifted from 36.86° to 36.78° after introduction of S atoms, indicating the expansion of (311) lattice spacing in the presence of S atoms.
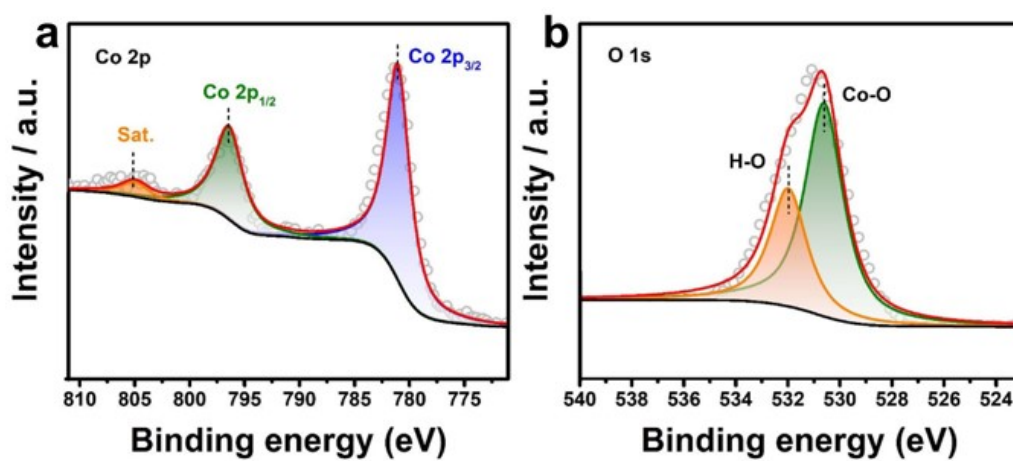

Fig. S6. XPS results of Co 2p (a), and O 1s (b) of the pristine Co_3O_4 sample.
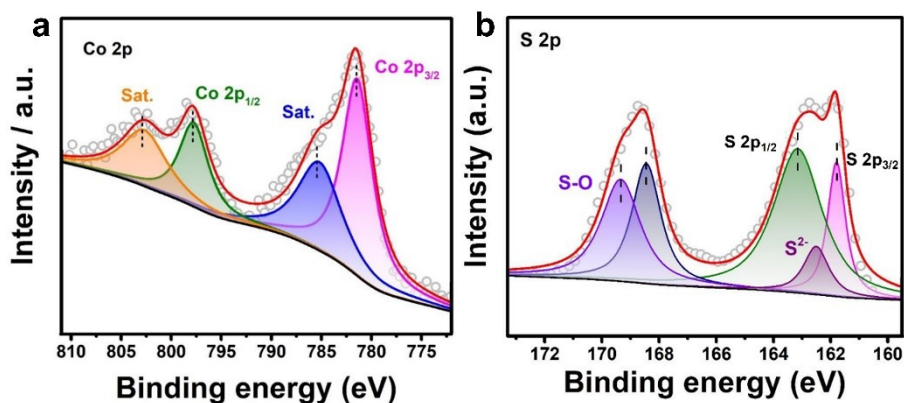
Fig. S7. XPS results of Co 2p (a), and S 2p (b) of the CoS_2 sample.
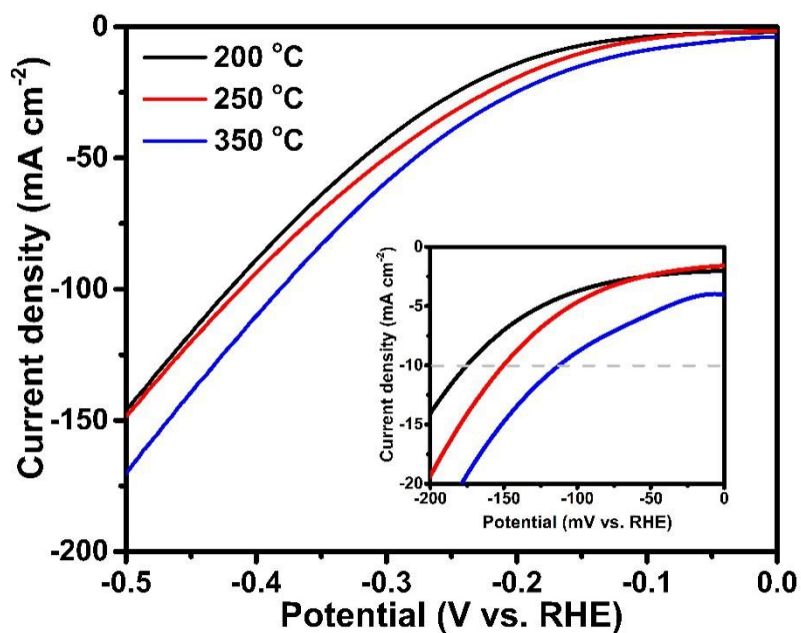

Fig. S8. LSV curves of the partially sulfurized samples obtained from 200, 250, and 350 °C. The inset is a magnified LSV region that shows the current density of 10 mA cm^{-2}.

The LSV curves reveal that OP@10 mA cm^{-2} decreases when the sulfurization temperature increases, which is consistent with the ESR results of Fig. 3d.

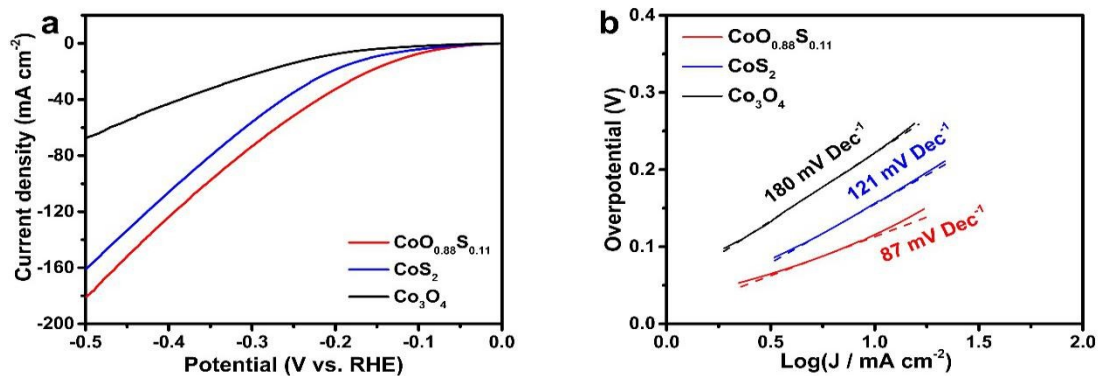**Fig. S9.** LSV curves (a) , and Tafel plots (b) of the $CoO_{0.88}S_{0.11}$, CoS_2, and Co_3O_4 samples, respectively. The electrolyte used is 0.5 M of H_2SO_4 aqueous solution.
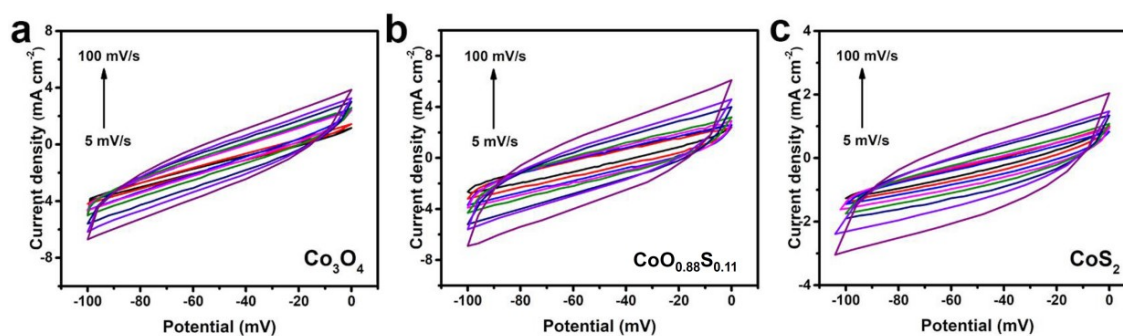

Fig. S10. CV curves obtained from various scan rates with the same non-Faradaic potential region of -0.1 - 0 V (vs. SCE) for all the three samples.

The CV measurements were performed within a non-Faradaic potential region to estimate the electrochemical double-layer capacitance.
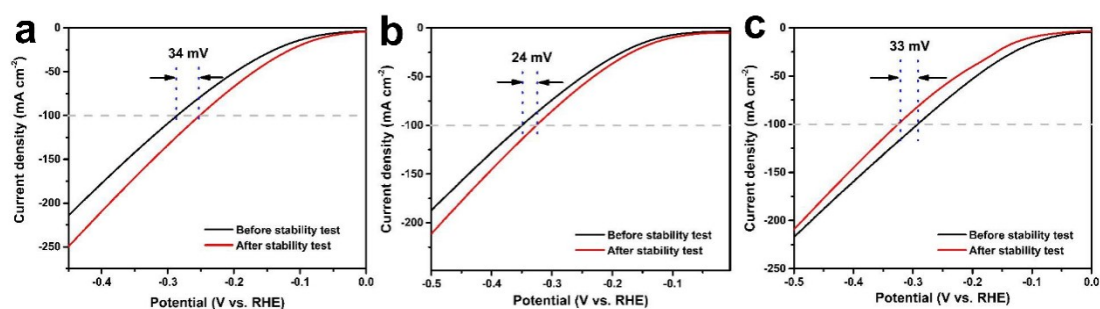
Fig. S11. LSV curves obtained before and after stability tests (for 12 h) for the samples Co_3O_4 (a), $CoO_{0.88}S_{0.11}$ (b), and CoS_2 (c), respectively.

The overpotential differences ($\Delta\eta = OP_{after} - OP_{before}$) of η_{100} are -34, -24, and 33 mV for the samples Co_3O_4, $CoO_{0.88}S_{0.11}$, and CoS_2, respectively. The results indicate that the catalytic activities for Co_3O_4 and $CoO_{0.88}S_{0.11}$ are improved after stability tests, but deteriorated for CoS_2.

Table S1. Comparison table of the previously reported electrocatalysts for HER.

Catalysts	Electrolyte	Morphology	η_{10} (mV)	Tafel slope (mV Dec^{-1})	Ref.
$CoO_{0.88}S_{0.11}$	1 M KOH	spheres	83	80	this work
$CoO_{0.88}S_{0.11}$	0.5 M H_2SO_4	spheres	116	87	this work
CoS@CoNi-LDH/CC	1 M KOH	nanorods	124	89	1
Co_3S_4	1 M KOH	nanosheets	163	103	2
meso CoSSe	0.5 M H_2SO_4	spheres	110	52	3
$Ru/Ti_3C_2T_x$	0.1 M $HClO_4$	nanosheets	70	76	4
$CoSe_2$	1 M KOH	nanotubes	124	66	5
Co_9S_8/CC	0.5 M H_2SO_4	nanosheets	150	-	6
$Co(S_{0.73}Se_{0.27})_2$	0.5 M H_2SO_4	nanowires	104	45	7
CoS_2/RGO-CNT	0.5 M H_2SO_4	nanosheets	142	51	8

References

1. ACS Applied Materials & Interfaces, 2020, 12, 33595-33602.

2. ACS Catalysis, 2018, 8, 8077-8083.

3. ACS Catalysis, 2019, 9, 456-465.

4. Small, 2020, 16, 2002888. (Note: **Ru metal was used!**)

5. Journal of Materials Chemistry A, 2017, 5, 4513-4526.

6. Journal of Materials Chemistry A, 2016, 4, 6860–6867.

7. Nano Energy, 2015, 18, 1-11.

8. Angewandte Chemie International Edition, 2014, 126, 12802 -12807.